SIMULATION OF HEAT TRANSFER AND METAL FLOW IN WIRE-BASED ELECTRO BEAM ADDITIVE MANUFACTURING

ALEXEY V. SHCHERBAKOV, DARIA A. GAPONOVA, REGINA V. RODYAKINA, ALEXANDER V. GUDENKO, ANDREY P. SLIVA, VIKTOR P. RUBTSOV AND VIKTOR K. DRAGUNOV

National Research University "Moscow Power Engineering Institute (MPEI)"
Krasnokazarmennaya 14, 111250 Moscow, Russia
e-mail: ShcherbakovAV@mpei.ru, web page: http://mpei.ru

Key words: Metal Wire Deposition, Electron Beam Melting, Navier-Stokes Equations, Metal Flow, Finite Difference Method, Surface Tension, Electron Beam Sweep

Abstract. The urgency of mathematical model development for wire-based electron-beam additive manufacturing process analysis is shown. The procedure of solving heat equation for metal in the solid phase and the Navier-Stokes equations in the liquid phase, based on the use of the finite-difference method and the predictor-corrector procedure is described. An algorithm for numerical approximation of free melt surface motion, using the concept of the volume of fluid (VOF), is described as well. A numerical algorithm for surface tension force calculating is proposed. The model described above was realized as a program in the Microsoft Visual Studio environment. Series of computational experiments were carried out to calculate metal flow during deposition with the use of 316L steel wire. The results of experiments are compared with experimental data.

1 INTRODUCTION

Wire-based electron-beam additive manufacturing (also known as electron beam freeform fabrication, EBF^3 [1]) meets the requirements for structure and quality of formed metal layer, since the whole process is realized in vacuum (10^{-3}...10^{-5} Torr), and size and shape of heat source can be varied by the use of magnetic deflection coils. Usually, wire with a diameter of 0.8 to 2.4 mm is used, and the wire feed rate is 3-5 times higher than the deposition rate. The minimum width of deposit layer for this process is 6-8 mm, what determines the spatial resolution of this technology. Typical for the technology process performance for large-sized products with dimensions of 500 mm and more can vary from 3 to 12 kilograms of metal per hour [2]. Today, it is too early to talk about the wide industrial use of the technology. Control of metal transfer mode, which is influenced by many factors, remains an unsolved problem, and is primarily associated with inconstancy of heat transfer conditions. Experimental methods such as high-speed imaging in visible or infrared optical range can be used to control the mode of metal flow. These methods provide indirect information, such as temperature distribution over the observed surface or bead shape in the deposition process. Moreover, these methods require expensive equipment and many series of experiments. Therefore, predicting the results of surfacing using experimental studies will be a time-consuming process. To obtain information about velocity distribution and pressure, as well as temperature distribution over the depth of weld pool, it is necessary to use methods of mathematical modelling.

2 MODEL DESCRIPTION

A graphical representation of the model is shown in Fig. 1. Wire is fed with the rate of v_{wire} to the area in which electron beam is applied. Metal melts and flows onto the substrate, forming a bead. Electron gun moves with wire feeder at a given speed. Heat and mass transfer in the system "electron beam –wire – substrate" should be described in a formulation that takes into account the flow of metal under the action of pressure field, gravity, and forces due to viscosity and surface tension. For this, it is necessary to use the Navier-Stokes equations, which describe the flow of a viscous incompressible fluid, and include, firstly, the continuity equation

$$\frac{\partial v_x}{\partial x} + \frac{\partial v_y}{\partial y} + \frac{\partial v_z}{\partial z} = 0, \tag{1}$$

where v_x, v_y and v_z are the projections of velocity vector on the x, y and z axes.

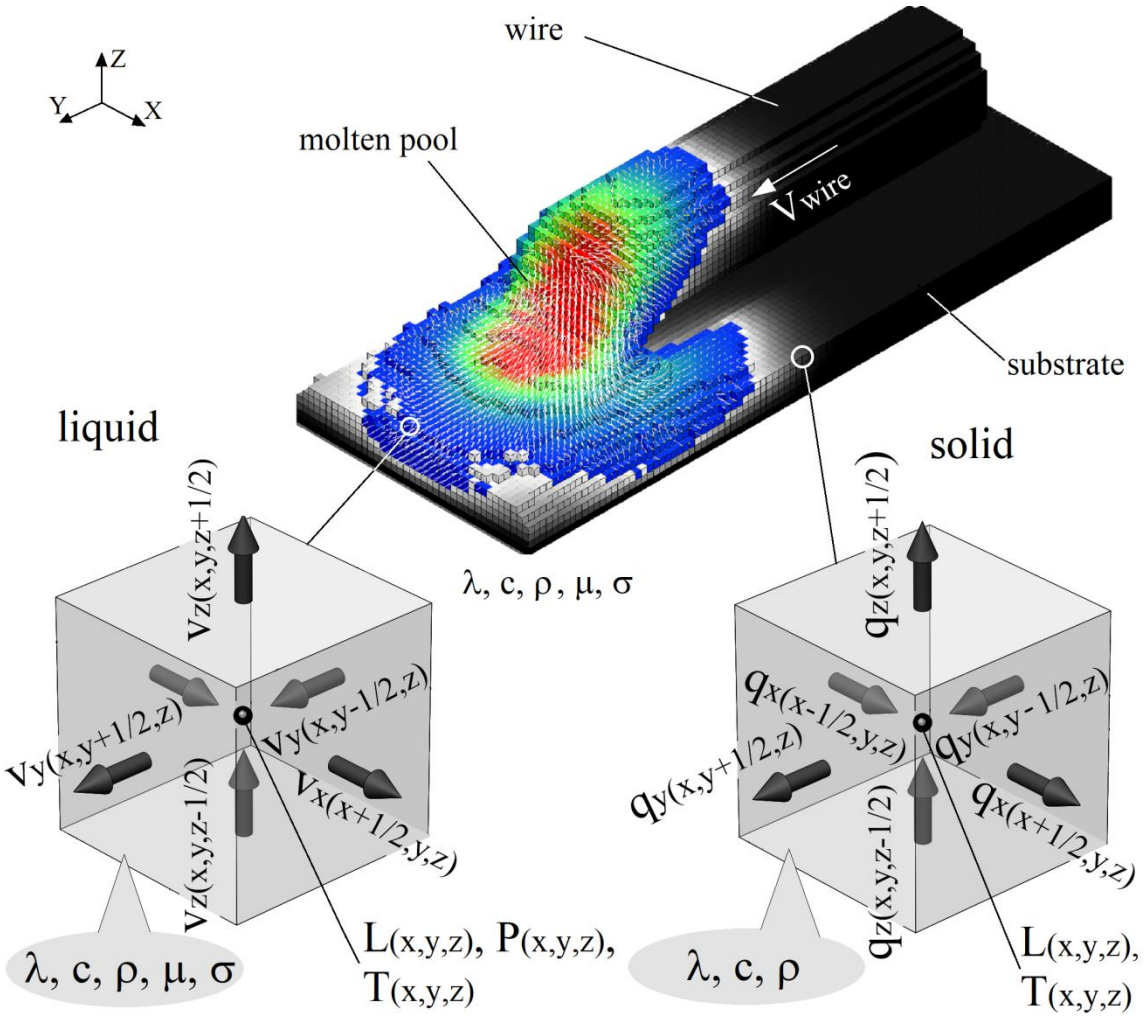

Figure 1: Surfacing process presented in accordance with the concept of cubic control volumes

Secondly, the system includes the momentum equation, which written in projection form

$$\frac{\partial v_x}{\partial t} + v_x \frac{\partial v_x}{\partial x} + v_y \frac{\partial v_x}{\partial y} + v_z \frac{\partial v_x}{\partial z} = -\frac{1}{\rho}\frac{\partial P}{\partial x} + \mu\left(\frac{\partial^2 v_x}{\partial x^2} + \frac{\partial^2 v_x}{\partial y^2} + \frac{\partial^2 v_x}{\partial z^2}\right) + \frac{1}{\rho}\sigma\kappa\frac{dL}{dx};$$

$$\frac{\partial v_y}{\partial t} + v_x \frac{\partial v_y}{\partial x} + v_y \frac{\partial v_y}{\partial y} + v_z \frac{\partial v_y}{\partial z} = -\frac{1}{\rho}\frac{\partial P}{\partial y} + \mu\left(\frac{\partial^2 v_y}{\partial x^2} + \frac{\partial^2 v_y}{\partial y^2} + \frac{\partial^2 v_y}{\partial z^2}\right) + \frac{1}{\rho}\sigma\kappa\frac{dL}{dy}; \quad (2)$$

$$\frac{\partial v_z}{\partial t} + v_x \frac{\partial v_z}{\partial x} + v_y \frac{\partial v_z}{\partial y} + v_z \frac{\partial v_z}{\partial z} = -\frac{1}{\rho}\frac{\partial P}{\partial z} + \mu\left(\frac{\partial^2 v_z}{\partial x^2} + \frac{\partial^2 v_z}{\partial y^2} + \frac{\partial^2 v_z}{\partial z^2}\right) + \frac{1}{\rho}\sigma\kappa\frac{dL}{dz} - g,$$

where P is pressure, Pa; μ is kinematic viscosity, m^2/s, t is time, s; g is gravity acceleration, m/s^2, ρ is density, kg/m^3, σ is surface tension coefficient, J/m^2, κ is curvature index, 1/m, L is dimensionless function of filling the control volume with fluid, $0 < L < 1$. At $L = 1$, the control volume is filled with fluid, and at $L = 0$ it is empty. This method is known as the Volume of Fluid (VOF) method, and it has proven itself for solving hydrodynamic problems [3, 4]. The VOF concept used in the model is illustrated by Figure 2.

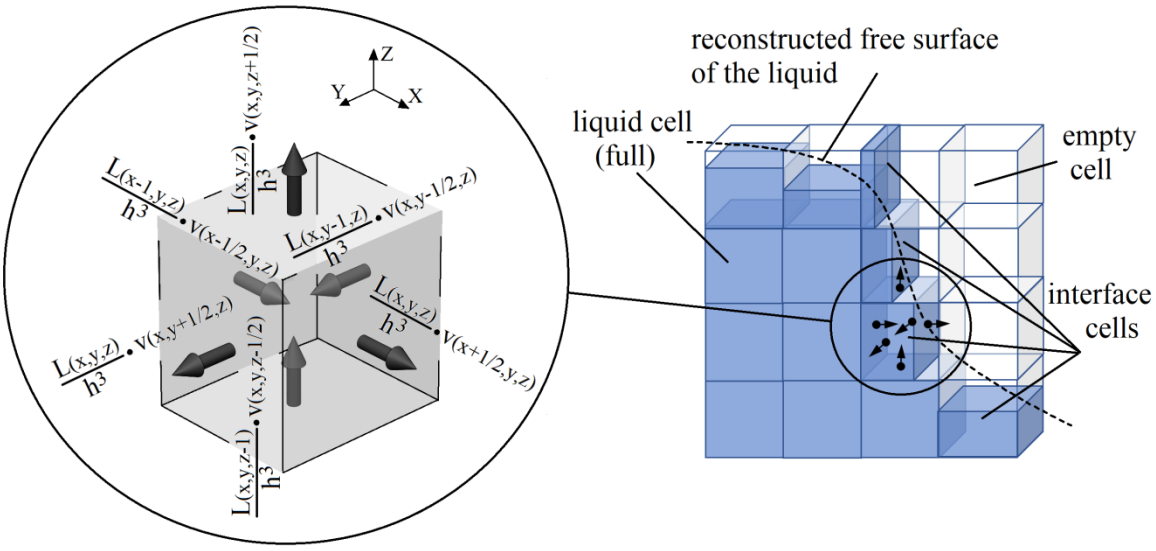

Figure 2: VOF concept used in the proposed model: h^3 is the volume of full liquid cell (sides of a cubic cell had a size h)

In accordance with this method, the flow of fluid between the control volumes is described by means of equation

$$\frac{\partial L}{\partial t} + v_x \frac{\partial L}{\partial x} + v_y \frac{\partial L}{\partial y} + v_z \frac{\partial L}{\partial z} = 0. \quad (3)$$

In cells with $\nabla L \neq 0$, surface tension forces (see eq. 2) acts to prevent the free surface from stretching. These forces depend on temperature and free surface curvature.

Heat transfer in a liquid pool is carried out due to convection and heat conduction and it is described by the energy equation

$$\frac{\partial T}{\partial t} + v_{\mathrm{x}}\frac{\partial T}{\partial x} + v_{\mathrm{y}}\frac{\partial T}{\partial y} + v_{\mathrm{z}}\frac{\partial T}{\partial z} = \frac{\lambda}{c\rho}\left(\frac{\partial^2 T}{\partial x^2} + \frac{\partial^2 T}{\partial y^2} + \frac{\partial^2 T}{\partial z^2}\right) + \frac{Q_{\mathrm{v}}}{c\rho}. \quad (4)$$

In the last equation, T is temperature, K, c is specific heat capacity, J/(kg·K), Qv is volume representation of electron beam energy released in the control volume as a heat, W/m^3. Heat transfer in the solid phase is described by the equation of heat conductivity (the projections of heat flux vectors between cubic cells are shown in Fig. 1 as q_{x}, q_{y} and q_{z})

$$\frac{\partial T}{\partial t} = \frac{\lambda}{c\rho}\left(\frac{\partial^2 T}{\partial x^2} + \frac{\partial^2 T}{\partial y^2} + \frac{\partial^2 T}{\partial z^2}\right) + \frac{Q_v}{c\rho} - H_m \cdot \rho\frac{\partial \psi_m}{\partial t}, \quad (5)$$

where H_{m} is latent heat of fusion of metal, J/kg; $\psi_{\mathrm{m}}(\mathrm{T})$ is relative amount of fluid in the control volume, calculated with using equation

$$\psi_{\mathrm{m}}(T) = \begin{cases} 0, & T < T_{\mathrm{S}} \\ \dfrac{T - T_{\mathrm{S}}}{T_{\mathrm{L}} - T_{\mathrm{S}}}, & T_{\mathrm{S}} < T < T_{\mathrm{L}} \\ 1, & T > T_{\mathrm{L}} \end{cases}. \quad (6)$$

In the equation (6) T_{S} and T_{L} are, respectively, solidus and liquidus temperatures of the material being remelted, K.

Now it is necessary to describe the boundary conditions. Stefan-Boltzmann condition is set on surfaces facing vacuum

$$q_{\perp} = -\varepsilon \cdot k \cdot \left(T_{surface}^4 - T_{chamber}^4\right), \quad (7)$$

where ε is the total emissivity for the radiating surface, $k = 5.67 \cdot 10^{-8}$ W/(m^{2}K^4) is the Stefan-Boltzmann constant, T_{surface} is the surface temperature and T_{chamber} is vacuum chamber temperature, which is assumed to be 25°C. A heat transfer condition by heat conduction into the fixture was proposed for the substrate bottom surface

$$q_{\perp} = -\lambda_{fix}\frac{T_{surface} - T_{chamber}}{\mathrm{S}_{fix}}, \quad (8)$$

where $\lambda_{\mathrm{fix}} = 400$ W/(m·K) is the thermal conductivity of a copper fixture and S_{fix} is the fixture thickness, which is assumed to be 0.02 meters. Heat source was represented by volumetric function Q_{v}, which depends on z according to the equation

$$Q_v = \begin{cases} 0, & z < z_{\mathrm{surface}} \\ \dfrac{1}{\pi \cdot r_{\mathrm{eff}}^2} I_b U_a exp\left(\dfrac{-\left(\left(x - x_{\mathrm{pos}}(t)\right)^2 + \left(y - y_{\mathrm{pos}}(t)\right)^2\right)}{r_{\mathrm{eff}}^2}\right)\dfrac{1}{dz}, & z = z_{\mathrm{surface}} \\ 0, & z > z_{\mathrm{surface}} \end{cases}. \quad (9)$$

In the equation (9) z_{surface} is z-coordinate of control volume in which electrons energy is converted into heat; I_{b} is beam's current, A; U_{a} is accelerating voltage, V; x_{pos}, y_{pos} are the current values of electron beam center coordinates (depends on time t), m; r_{eff} is beam effective radius (assumed to be 0.2-0.5 mm), m; dz is z-size of the control volume in which

electron beam heating is effected, m.

The most complex boundary conditions for the momentum equation are given on the free surfaces of liquid metal. The acceleration due to the action of surface tension forces is described in the momentum equation (2) and appears only when a gradient of the function L exists. The vapor recoil pressure (Pa) can be described by the Antoine equation as

$$P_{recoil} = 133 \cdot 10^{8.8-18700/T_{surface}} \tag{10}$$

and the acceleration due to this pressure, m/s^2

$$a_{recoil} = P_{recoil} \frac{\nabla L}{L|\nabla L|} \frac{1}{\rho h} \tag{11}$$

where ∇L is the gradient of function L, which appears on the surfaces. The pressure outside the metal (in the empty cells with L=0) is assumed to be equal to the vacuum chamber pressure (in these experiments the chamber pressure was 0.1 Pa)

$$P_{(L=0)} = P_{chamber} \tag{12}$$

On the boundary between liquid and solid metal there is the condition

$$v_L = v_S, \tag{13}$$

where index L refers to the liquid phase, and index S refers to the solid phase. For example, if the wire moves at a speed v_{wire}, then metal's velocity flow at the wire's melting boundary will also be equal to v_{wire}.

The physical properties of metal are temperature dependent. To account for data dependencies for steel 316L were collected literature data [5, 6, 7, 8]. Figure 3 shows the dependencies used in the development of heat and mass transfer model.

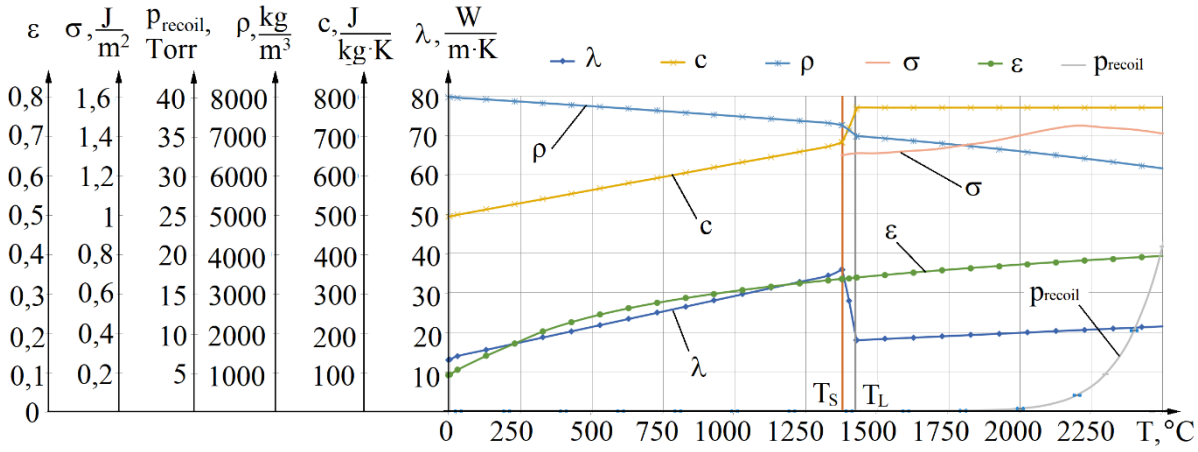

Figure 3: Physical properties of steel 316L vs temperature

3 NUMERICAL MODEL IMPLEMENTATION AND SOME ALGORITHMS

To solve the system of equations (1)–(13), the finite difference method and a fixed grid with cubic cells were used. This grid has "staggered" structure [9]. In such a grid, the nodes, in which velocities are calculated, are displaced along all three axes by half the coordinate

step relative to the nodes in which there are calculated pressure P, function of cell's filling L and fluid temperature T (Fig. 1). The grid spacing was taken to be $h = 0.05…0.1$ mm, and the time interval was $5\cdot10^{-6}…1{,}25\cdot10^{-5}$ s. At the current stage of research, an explicit difference scheme was used with fixed coordinate and time steps.

At the beginning of heating process, melting does not occur, so it is necessary to solve the equation (5). For example, to calculate the temperature in the current coordinate node at time moment $t + 1$, we used the following finite-difference approximation of equation (5):

$$T_{(x,y,z)}^{t+1} = T_{(x,y,z)}^{t} + \Delta t\left(\frac{\lambda}{c\rho}\left(\frac{T_{(x+1,y,z)}^{t} - 2T_{(x,y,z)}^{t} + T_{(x-1,y,z)}^{t}}{h^2} + \right.\right. \\ \left.\left. + \frac{T_{(x,y+1,z)}^{t} - 2T_{(x,y,z)}^{t} + T_{(x,y-1,z)}^{t}}{h^2} + \frac{T_{(x,y,z+1)}^{t} - 2T_{(x,y,z)}^{t} + T_{(x,y,z-1)}^{t}}{h^2}\right) + \frac{Q_v}{c\rho}\right) \tag{14}$$

After reaching the temperature T_L in the control volume metal was considered to be molten and the system of equations (1)–(4) must be solved. For the numerical calculation of pressure and velocity fields (equations 1 and 2), a method proposed by S. Patankar [9] was used. At the first time step, velocity field is assumed known (all velocities are zero). Velocity increments were calculated by equation (2) without taking into account values of pressure (predictor step). For example, the x-projection of velocity was calculated according to the equation

$$v_{x(x,y,z)}^{t(t+1)_{predictor}} = v_{x(x,y,z)}^{t} + \Delta t \times \\ \times\left(-v_{x(x,y,z)}^{t}\cdot\frac{v_{x(x+1,y,z)}^{t} - v_{x(x-1,y,z)}^{t}}{2h} - v_{y(x,y,z)}^{t}\cdot\frac{v_{x(x,y+1,z)}^{t} - v_{x(x,y-1,z)}^{t}}{2h} - v_{z(x,y,z)}^{t}\cdot\frac{v_{x(x,y,z+1)}^{t} - v_{x(x,y,z-1)}^{t}}{2h} + \right. \\ +\mu\left(\frac{v_{x(x+1,y,z)}^{t} - 2v_{x(x,y,z)}^{t} + v_{x(x-1,y,z)}^{t}}{h^2} + \frac{v_{y(x,y+1,z)}^{t} - 2v_{y(x,y,z)}^{t} + v_{y(x,y-1,z)}^{t}}{h^2} + \frac{v_{z(x,y,z+1)}^{t} - 2v_{z(x,y,z)}^{t} + v_{z(x,y,z-1)}^{t}}{h^2}\right) + \\ \left. + \frac{1}{\rho}(\sigma\kappa + p_{recoil})\frac{L_{(x+1,y,z)}^{t} - L_{(x-1,y,z)}^{t}}{2h}\right). \tag{15}$$

Then, the scalar pressure field in the liquid metal (step-corrector) was calculated using the method described in [9,10,11]. The pressure was calculated by the Poisson equation, which satisfies the continuity equation (1)

$$\frac{\partial^2 P}{\partial x^2} + \frac{\partial^2 P}{\partial y^2} + \frac{\partial^2 P}{\partial z^2} = \frac{\rho}{\Delta t}\cdot\left(\frac{\partial v_x}{\partial x} + \frac{\partial v_y}{\partial y} + \frac{\partial v_z}{\partial z}\right). \tag{16}$$

The resulting pressure field is necessary to adjust the velocity field. All values on the right side of the equation are constants for the considered time step (the velocities are calculated at the predictor step). Equation (16) was solved with using simple iteration method by expressing the pressure in the (x,y,z) node (in the center of cell) through the pressures in the surrounding cells and the derivatives of velocities calculated in displaced grid nodes

$$P_{(x,y,z)} = \frac{1}{6}\left(P_{(x+1,y,z)} + P_{(x-1,y,z)} + P_{(x-1,y,z)} + P_{(x,y+1,z)} + P_{(x,y-1,z)} + P_{(x,y,z+1)} + P_{(x,y,z-1)}\right. \\ \left. - \frac{h^2\rho}{6\Delta t}\left(\frac{v_{x\left(x+\frac{1}{2},y,z\right)} - v_{x\left(x-\frac{1}{2},y,z\right)}}{h} + \frac{v_{y\left(x,y+\frac{1}{2},z\right)} - v_{y\left(x,y-\frac{1}{2},z\right)}}{h} + \frac{v_{z\left(x,y,z+\frac{1}{2}\right)} - v_{z\left(x,y,z-\frac{1}{2}\right)}}{h}\right)\right). \tag{17}$$

After pressure field finding, the acceleration projections due to its action were calculated and the velocity field was corrected. For example, for velocity projection on the *x*-axis we have the following equation:

$$v_{x(x,y,z)}^{(t+1)_{corrector}} = v_{x(x,y,z)}^{(t+1)_{predictor}} + \left(-\frac{1}{\rho}\frac{P_{(x+1,y,z)}-P_{(x-1,y,z)}}{2h}\right)\Delta t. \quad (18)$$

In the liquid phase, thermal conductivity and convection will be simultaneously present, and the numerical form of heat transfer equation will be written as follows

$$T_{(x,y,z)}^{t+1} = T_{(x,y,z)}^{t} + \Delta t \times$$
$$\times\left(\frac{\lambda}{c\rho}\left(\frac{T_{(x+1,y,z)}^{t} - 2T_{(x,y,z)}^{t} + T_{(x-1,y,z)}^{t}}{h^2} + \frac{T_{(x,y+1,z)}^{t} - 2T_{(x,y,z)}^{t} + T_{(x,y-1,z)}^{t}}{h^2} + \frac{T_{(x,y,z+1)}^{t} - 2T_{(x,y,z)}^{t} + T_{(x,y,z-1)}^{t}}{h^2}\right) - \quad (19)$$
$$-v_{x(x,y,z)}^{t}\cdot\frac{T_{\left(x+\frac{1}{2},y,z\right)}^{t} - T_{\left(x-\frac{1}{2},y,z\right)}^{t}}{h} - v_{y(x,y,z)}^{t}\cdot\frac{T_{\left(x,y+\frac{1}{2},z\right)}^{t} - T_{\left(x,y-\frac{1}{2},z\right)}^{t}}{h} - v_{z(x,y,z)}^{t}\cdot\frac{T_{\left(x,y,z+\frac{1}{2}\right)}^{t} - T_{\left(x,y,z-\frac{1}{2}\right)}^{t}}{h} + \frac{Q_v}{c\rho}\Bigg).$$

After that, it is necessary to simulate the motion of free surface, and also to determine the fields of surface tension force. The finite difference approximation of equation (3) for the case, if no additional conditions are specified, should have the following form

$$L_{(\mathrm{x,y,z})}^{t+1} = L_{(\mathrm{x,y,z})}^{t} + \Delta t \times \Bigg(\frac{L_{\left(\mathrm{x}+\frac{1}{2},\mathrm{y,z}\right)}^{t} v_{\mathrm{x}\left(\mathrm{x}+\frac{1}{2},\mathrm{y,z}\right)}^{t} - L_{\left(\mathrm{x}-\frac{1}{2},\mathrm{y,z}\right)}^{t} v_{\mathrm{x}\left(\mathrm{x}-\frac{1}{2},\mathrm{y,z}\right)}^{t}}{h} +$$
$$+\frac{L_{\left(\mathrm{x,y}+\frac{1}{2},\mathrm{z}\right)}^{t} v_{\mathrm{y}\left(\mathrm{x,y}+\frac{1}{2},\mathrm{z}\right)}^{t} - L_{\left(\mathrm{x,y}-\frac{1}{2},\mathrm{z}\right)}^{t} v_{\mathrm{y}\left(\mathrm{x,y}-\frac{1}{2},\mathrm{z}\right)}^{t}}{h} + \frac{L_{\left(\mathrm{x,y,z}+\frac{1}{2}\right)}^{t} v_{\mathrm{z}\left(\mathrm{x,y,z}+\frac{1}{2}\right)}^{t} - L_{\left(\mathrm{x,y,z}-\frac{1}{2}\right)}^{t} v_{\mathrm{z}\left(\mathrm{x,y,z}-\frac{1}{2}\right)}^{t}}{h}\Bigg) = \quad (20)$$
$$= L_{(\mathrm{x,y,z})}^{t} + \Delta t\cdot\Omega.$$

However, a direct numerical solution of such a system can lead to the appearance of anomalous results, since this approach does not take into account that function *L* in each control volume should always take values in the range from 0 to 1. This circumstance led to the creation of various methods for solving equation (3), described in the literature [3, 10,11,12]. In this work, the sign of velocity and magnitude of flux flowing into the control volume, or, on the contrary, flowing from it, was tracked. In the case of control volume overflow, or, on the contrary, its emptying, a proportional decrease in the stream was made to prevent function *L* value output out of the interval [0…1].

In addition to the above conditions introduced into the algorithm for solving equation (20), the calculation of the function *L* distribution was carried out iteratively with fragmentation of time step. The maximum fractional step Δt_{frac} was selected from the condition

$$\Delta t_{\mathrm{frac}}\cdot\max\Omega \le 0.1. \quad (21)$$

The next step was the calculation of surface tension forces. The normal to the free surface was calculated as function gradient *L* direction, and the sign and magnitude of the force were

calculated from the surface curvature κ (see eq. 2 and eq. 15). The curvature index was determined as follows. In the computational grid, a spherical region with a center at the point under consideration (*x*,*y*,*z*) lying on the free surface was distinguished (Fig. 4).

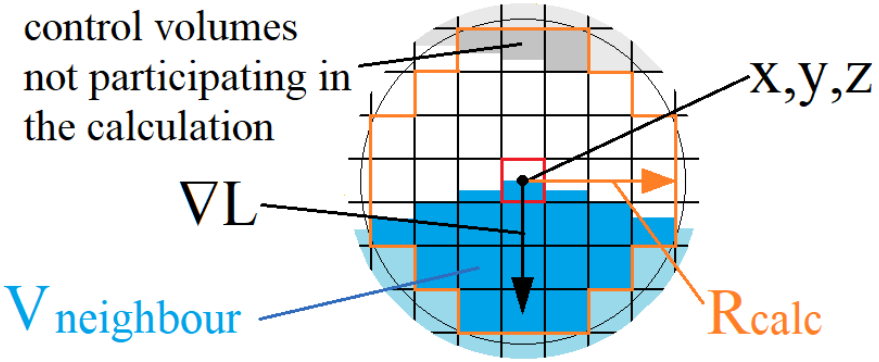

Figure 4: To the calculation of curvature index of the surface

The region has radius R_{calc} (this value determines the accuracy of calculation, we took 4-6 grid points). Then, by summing the volumes inside the sphere ($V_{\text{neighbour}}$ shown in Fig. 2) we calculated the curvature index from geometric considerations by means of equation

$$\kappa = -\frac{12V_{\text{neighbour}} - 8\pi R_{\text{calc}}^3}{3\pi R_{calc}^4} \tag{22}$$

This algorithm was implemented only for cells in which $\nabla L \neq 0$, the direction of ∇L is similar with the direction of surface tension force, and the force sign depends on the surface curvature sign. Since the surface tension force contains the derivative of function L, this allows to provide the "compression" of free surface and eliminates its "blurring", which is typical for the VOF-algorithms described by equation (3).

4 TEST PROBLEMS AND VERIFICATION

At the first stage, melting of a fixed wire with beam power of 800 W oscillating at a frequency of 400 Hz around a circular trajectory with the radius of 0.8 mm and moving along the wire at a speed of 20 mm/s was simulated. The effective beam radius was assumed to be 0.8 mm. The simulation results are graphically shown in Fig. 5.

Caption *a*,*b*...*e* in Fig. 5 corresponds to different time points: *a* – 2.75 ms; *b* – 31.25 ms; *c* – 93.75 ms; *d* – 125 ms and *e* – 375 ms. Beam position at these points is shown by dashed line (marked by number 1). For the entire period electron beam moves at a distance of 7.5 mm, making 150 oscillations along a circular path with a radius of 0.8 mm (sweep radius).

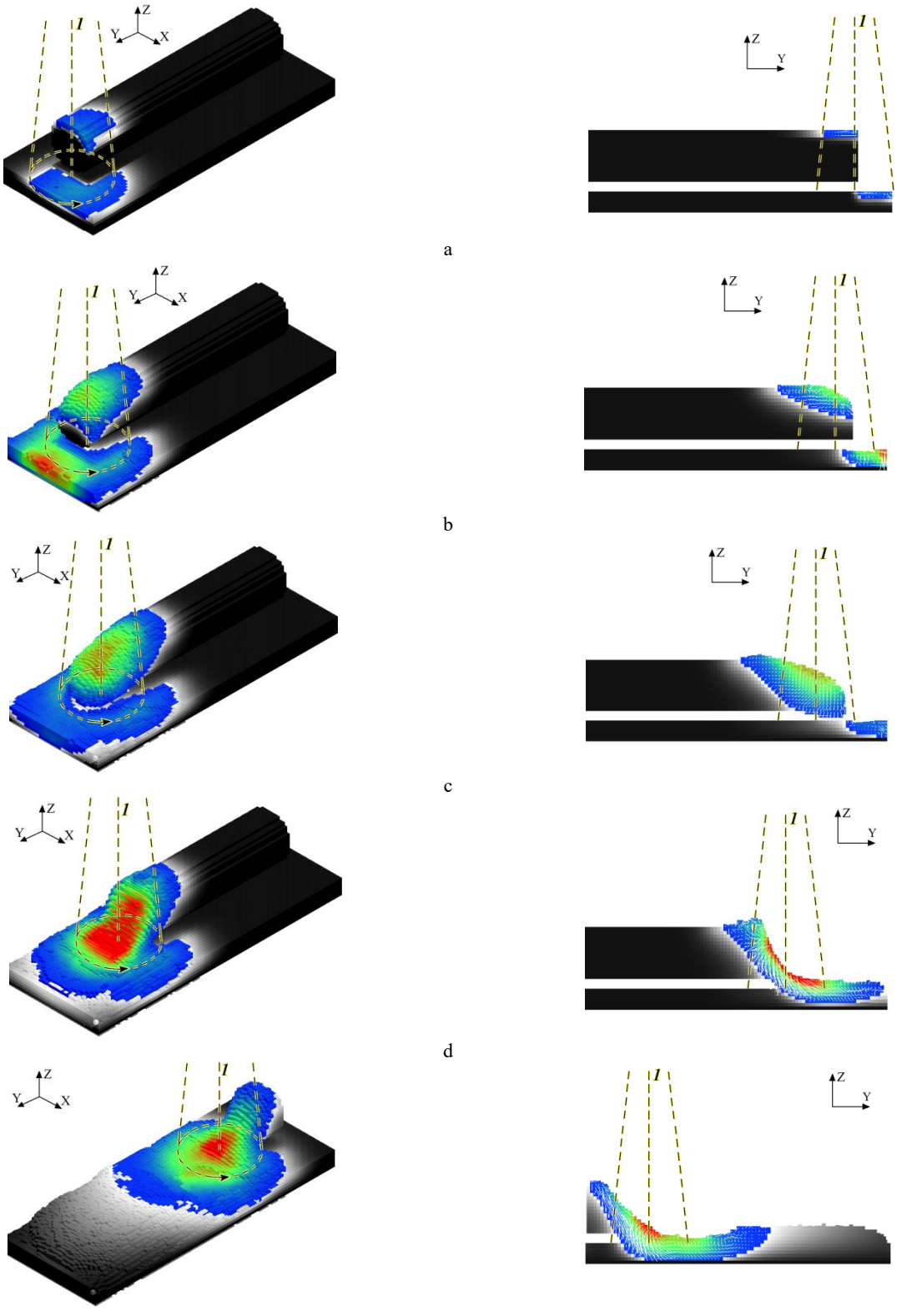

Figure 5: Simulation results at a different time moments

The flow is almost laminar: metal flows mainly due to gravity, and turbulence is observed only in the tail part of liquid pool, and it is caused by interaction of the flow with a solid bead wall. The maximum flow velocity calculated during the transition to stationary mode of transfer was recorded in the central part of metal jet and amounted to 0.68 m/s. The bead shape (ratio of height to width) corresponds to published literature data [13]. It is reasonable to assume that an increase in the rate of metal flow due to an increase in the wire feed rate (and, correspondingly, beam power) may lead to an intensification of the process of forcing the fluid to the top.

It is also obvious that reducing beam sweep radius will reduce width of molten area on the substrate, which in turn should lead to the formation of a narrower and higher bead. Fig. 6 shows the use of a narrow beam sweep, in which virtually all power is released in an area not exceeding the wire itself. In this example, the wire diameter is 0.8 mm, the sweep radius is 0.15 mm and the beam radius is 0.2 mm. The wire moves at a speed of 7.5 mm/s relative to the substrate, and the oscillating beam moves in the opposite direction at a speed of 5 mm/s (deposition rate is 5 mm/s and equivalent wire feed rate is 12,5 mm/s). The frequency of beam oscillations was 600 Hz and electron beam power was 1 kW.

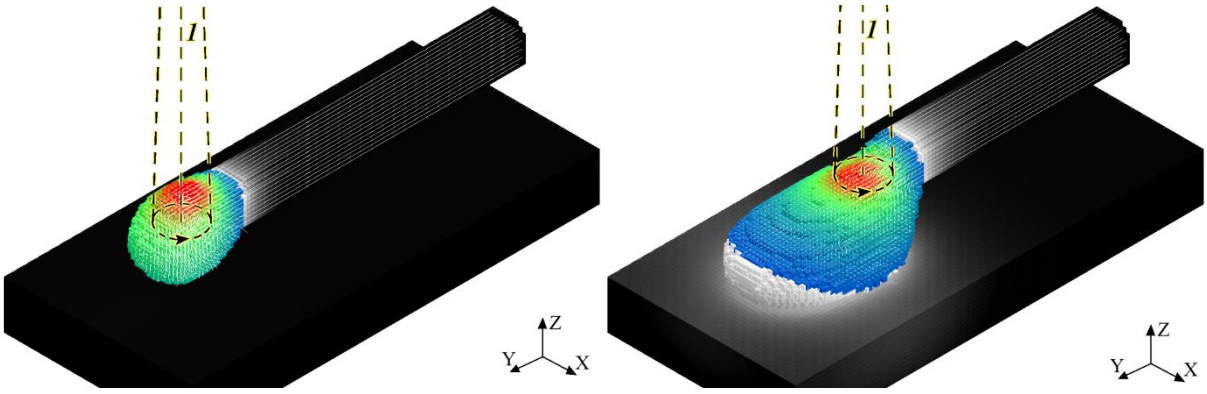

a b

Figure 6: Simulation results for the case of narrow beam oscillations

To verify the process, a mode was chosen that is implemented in the laboratory on the ELA-15I installation. The deposition rate was 5.6 mm/s, and the wire feed rate was 30 mm/s. The wire diameter was 1.2 mm, and the beam sweep radius was 0.6 mm (a wider scan was used than in the previous case). The beam power was 1.5 kW. Figure 7 shows the additive manufacturing modeling results with the single bead deposited with the above parameters. Fig. 7, a, shows velocity field and temperature field during depositing in stationary mode. It is seen that material feed rate has a significant impact on metal transfer in the molten pool. There are vortex flows in the upper and lower parts of the bead. As a result of metal displacement to the top, the pool height increases, and periodical nature of transfer leads to the appearance of ripples. Metal transfer in the lower part of the pool leads to the slope of molten pool. This example shows the differences in the nature of metal transfer when the wire feed rate exceeds the deposition rate. Fig. 7, b, shows a comparison of shape and size of weld bead obtained as a result of experiments (left) and modeling (right). It is seen that the forms

are similar to each other, there are slight differences in the height and shape of the upper part of the bead. The differences seem to be related to the discrete representation of computational domain and methods used for calculation. These data show that the model can be used to analyze the processes of wire-based additive manufacturing.

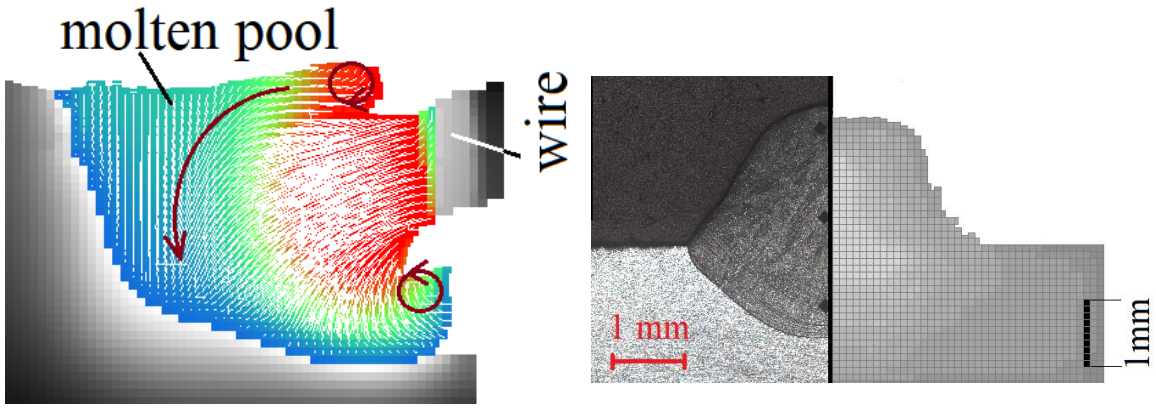

a b

Figure 7: Verification of results: velocity and temperature fields (a) and comparison of bead cross-section with experiment result (b)

5 CONCLUSIONS

- A model based on the use of a fixed offset grid and the VOF method, which allow to realize the simulation of wire-based additive manufacturing, has been proposed. It is shown that the model is distinguished by the possibility of taking into account temperature dependences of materials physical properties, surface tension forces and vapor recoil pressure, as well as the possibility of simulating heating by oscillating electron beam.
- It is shown that in the absence of wire movement (when beam moves relative to the wire), or at wire feed rate close to the deposition rate, the nature of metal transfer will be laminar, vortex flows may appear only near crystallization front, and their velocities are small. The maximum speed will be observed in the area of metal jet, and this speed was within 0.4-0.8 m/s.
- According to the results of simulation experiments, the effect of electron beam circular oscillation size on bead parameters was studied. It is shown that reducing the oscillation to values less than wire diameter allows to form a higher and narrow beads on the substrate.
- Verification of the process at a wire feed rate 5.6 times greater than deposition rate was carried out. A satisfactory coincidence of bead shape with experimental data was reached. With the help of the model, a significant change in metal transfer in the pool due to the formation of vortex flows in the upper and lower parts of the pool is shown.

6 ACKNOWLEDGMENTS

This work was carried out in National Research University «Moscow Power Engineering Institute»; it was supported by grant from the Russian Science Foundation (Project 17-79-20015).

REFERENCES

[1] K.M.B. Taminger, R.A. Hafley. Electron beam freeform fabrication: a rapid metal deposition process // Proceedings of third annual automotive composites conference. Society of Plastic Engineers, Troy, Michigan, USA; 2003. P. 9–10.

[2] I. Gibson, D. Rosen, B. Stucker. Additive Manufacturing technologies. 3D Printing, Rapid Prototyping, and Direct Digital Manufacturing/New York: Springer Science+Business Media, 2015, 498 p.

[3] C.W. Hirt, B.D. Nichols. Volume of fluid (VOF) method for the dynamics of free boundaries // Journal of Computational Physics, Volume 39, Issue 1, January 1981, Pages 201-225

[4] Noh, W.F.; Woodward, P. (1976). "SLIC (Simple Line Interface Calculation). In proceedings of 5th International Conference of Fluid Dynamics, edited by A. I. van de Vooren & P.J. Zandbergen". Lecture Notes in Physics. 59: 330–340.

[5] Choong S. Kim. Thermophysical Properties of Stainless Steels. Argonne National Laboratory, 1975.

[6] Tristan S. Hunnewell, Kyle L. Walton, Sangita Sharma, Tushar K. Ghosh, Robert V. Tompson, Dabir S. Viswanath & Sudarshan K. Loyalka. Total Hemispherical Emissivity of SS 316L with Simulated Very High Temperature Reactor Surface Conditions//Nuclear Technology,Volume 198, 2017, Issue 3, pp. 293-305. DOI: 10.13182/NT10-6

[7] Y. Wang, Q. Shi, and H.L. Tsai. Modeling of the Effects of Surface-Active Elements on Flow Patterns and Weld Penetration // Metallurgical and materials transactions B, volume 32B, February 2006, pp. 145-161

[8] T. DebRoy, H.L. Wei, J.S. Zuback, T. Mukherjee, J.W. Elmer, J.O. Milewski, A.M. Beese, A. Wilson-Heid, A. De, W. Zhang. Additive manufacturing of metallic components – Process, structure and properties // Progress in Materials Science 92 (2018) 112–224

[9] S.V. Patankar. Numerical Heat transfer and fluid flow. Series in computational methods in mechanics and thermal sciences, 1980

[10] Nikolaos A. Kampanis, John A. Ekaterinaris. A staggered grid, high-order accurate method for the incompressible Navier–Stokes equations // Journal of Computational Physics, Volume 215, Issue 2, 1 July 2006, Pages 589-613

[11] H.K. Versteeg, W. Malalasekera. An introduction to computational fluid dynamics: The finite volume method. Longman Scientific & Technical, 1995, 257 pp.

[12] Vinay R. Gopala, Berend G.M. van Wachem. Volume of fluid methods for immiscible-fluid and free-surface flows //Chemical Engineering Journal, Volume 141, Issues 1–3, 15 July 2008, Pages 204-221

[13] L. Wang. Microstructure and Mechanical Properties of Electron Beam Deposits of AISI 316L Stainless steel. ASME 2011 International Mechanical Engineering Congress & Expos7ition IMECE2011. November 11-17, 2011, Denver, Colorado, USA.